PAPER

Broadband unidirectional scattering in the transverse direction and angular radiation realized by using a silicon hollow nanodisk under a radially polarized beam

To cite this article: Fengxia Xue *et al* 2022 *J. Phys. D: Appl. Phys.* **55** 095111

IOP Publishing Journal of Physics D: Applied Physics
J. Phys. D: Appl. Phys. **55** (2022) 095111 (9pp) https://doi.org/10.1088/1361-6463/ac394c

Broadband unidirectional scattering in the transverse direction and angular radiation realized by using a silicon hollow nanodisk under a radially polarized beam

Fengxia Xue, Haihua Fan, Qiaofeng Dai, Haiying Liu* and Sheng Lan

Guangdong Provincial Key Laboratory of Nanophotonic Functional Materials and Devices, School of Information and Optoelectronic Science and Engineering, Guangzhou 510006, People's Republic of China

E-mail: hyliu@scnu.edu.cn

Received 15 September 2021, revised 6 November 2021
Accepted for publication 12 November 2021
Published 26 November 2021

Abstract

In recent years, directional scattering has been one of the most active research hotspots in the field of nanophotonics. Herein, we study the directional scattering properties of a silicon hollow nanodisk (SHND) illuminated by a tightly focused radially polarized beam. The induced strong longitudinal total electric dipole interferes with transverse magnetic dipole to achieve a highly-efficient transverse unidirectional scattering when the SHND is located at a specific position in the focal plane. Moreover, the manipulated unidirectional scattering in the transverse direction can be realized in the broad wavelength range from 581 nm to 656 nm. In addition, the unidirectional angular radiation towards all directions can be realized by adjusting the position of the SHND. Our research results are helpful for the design of nanophotonic devices that can manipulate the angular radiation direction, and have potential applications in sensing, optical communications, solar cells and other fields.

Keywords: transverse unidirectional scattering, broadband scattering, visible region, radially polarized beam, angular radiation

(Some figures may appear in colour only in the online journal)

1. Introduction

Directional scattering of nanoparticles has attracted more and more attention and been applied to various applications such as optical nanoantennas [1], photonic integrated circuits [2–4], biomedical detection [5, 6] and metasurface [7, 8]. Previously, various plasmonic i.e. metallic nanomaterials have been studied and exploited extensively for directional nanoantenna design, sensing and absorber design [9–14]. However, due to the high inherent absorption loss of plasmonic nanomaterials, the performance efficiency of plasmonic nanoantenna is low. Compared with plasmonic nanomaterials, high refractive index dielectric materials, such as silicon (Si), germanium (Ge), gallium arsenide (GaAs), exhibit low ohmic loss due to its low imaginary part of the refractive index in the visible and near-infrared region [15, 16]. In addition, this kind of material can provide greater freedom for the direction regulation of directional nanoantennas because they can simultaneously excite the electric and magnetic responses [17–19]. In recent years, silicon has been the most promising material for the implementation of all-dielectric resonant

* Author to whom any correspondence should be addressed.

nanophotonics and been applied to nonlinear nanophotonics such as second and third harmonic generation effects [20, 21].

High refractive index dielectric nanoparticles exhibit very interesting scattering characteristics due to the interference among internal multipole responses. For example, the zero backward or forward scattering can be achieved when the multipoles in nanoparticles meet the Kerker [15, 22] or generalized Kerker [23, 24]. Besides, transverse scattering is also dramatically significant and can be widely applied in displacement sensing, metasurfaces, directional antennas design and other fields [25, 26]. Previously, researchers have proposed that longitudinal dipole which is crucial to achieve transverse scattering can be excited using asymmetric structures such as V-shaped, asymmetric dimer and stair-like nanoantenna under linearly polarized light sources [27–29]. Furthermore, radially polarized beam (RPB) and azimuthally polarized beam (APB) also have been used to excite the longitudinal dipole in recent years [30–34]. It was found that transverse unidirectional scattering can be realized by using a single nanoparticle displaced appropriately away from the focal point of focused RPB or APB. The rapidly varying electromagnetic field within the focal plane of these beams enables electromagnetic responses in nanoparticles to satisfy transverse Kerker condition at a specific position [31, 32]. In addition, it is also important to achieve broadband unidirectional scattering for some applications such as nanoantennas [35, 36]. However, broadband transverse unidirectional scattering is still challenging. Moreover, it is also important to flexibly control the angular radiation of the unidirectional nanoantenna for various potential applications such as sensor, solar cell technology, optical communication and integrated optics [37–39].

In this paper, we propose a scheme to achieve manipulated broadband unidirectional scattering in the transverse direction and unidirectional angular radiation regulation based on the silicon hollow nanodisk (SHND) illuminated by the tightly focused RPB. The tightly focused RPB excites the strong longitudinal total electric dipole (TED) which interferes with the induced transverse magnetic dipole (MD) to achieve a highly-efficient transverse unidirectional scattering where the transverse Kerker condition is fulfilled. In addition, the wavelength width of the transverse unidirectional scattering can be enlarged as high as 75 nm in the visible region. Then, the directional manipulation of the unidirectional angular radiation from 0° to 360° can be realized when we change the position of the SHND within the focal plane.

2. Geometry, beam and theoretical model

In order to achieve transverse scattering, we propose a scheme as shown in figure 1(a), in which the SHND is illuminated by a tightly focused RPB with a diameter of 420 nm at the focal plane [40, 41]. In order to achieve unidirectional scattering in the visible region, the height of the SHND is $H = 200$ nm and the inner and outer radius are $R_{\text{in}} = 50$ nm, $R_{\text{out}} = 90$ nm respectively, as shown in the inset. In addition, the numerical aperture of the objective lens used to focus the RPB is 0.9 and the relative dielectric constant of Si comes from Palik [42]. The SHND is placed in a homogeneous air medium with $\varepsilon_d = 1$. In fact, some results have shown that the spectral features of the given nanostructure remain unchanged while all resonances acquire some red shift along the wavelength scale if silica is used as the substrate [43, 44]. In our simulation, the focal field distributions of RPB and results in near-field and far-field region can be obtained using COMSOL Multiphysics in the frequency domain.

Different from previous studies, the incident beam here is a cylindrical vector beam RPB instead of a linearly polarized beam. Figures 1(b)–(e) show the focal-plane electromagnetic field intensity distribution near focus of the tightly focused RPB calculated by the vector diffraction theory [45, 46]. For the tightly focused RPB, its longitudinal field component is a strong pure electric field $\mathbf{E}_z$ which reaches the maximum at the optical axis, exciting the longitudinal electric dipole in the SHND. Moreover, the transverse electric field $\mathbf{E}_t\,(|\mathbf{E}_t|^2 = |E_x|^2 + |E_y|^2)$and transverse magnetic field component $\mathbf{H}_t\,(|\mathbf{H}_t|^2 = |H_x|^2 + |E_y|^2)$ are radially polarized and azimuthally polarized, respectively. It can also be seen from figures 1(c) and (e) that both $\mathbf{E}_t$ and $\mathbf{H}_t$ near the optical axis enhance with the distance away from the optical axis where the intensity of $\mathbf{E}_t$ and $\mathbf{H}_t$ is equal to zero.

In order to understand the contributions of various electric and magnetic multipoles to the total scattering spectrum better, we adopt a Cartesian multipole decomposition method [47, 48]. The multipolar decomposition originates from the polarization $\mathbf{P} = \varepsilon_0\,(\varepsilon_p - \varepsilon_d)\,\mathbf{E}$, where $\mathbf{E}$ is the total electric field within the nanoparticle, ε_0, ε_p, ε_d are the free-space dielectric constant, relative permittivity of the nanoparticle and relative permittivity of the surrounding medium, respectively. In addition, the multipoles are located at the origin of the Cartesian coordinate system according to the nanoparticle's center of mass. The multipole moments can be obtained by the integration of the induced polarization currents over the volume of the nanoparticle. The electric dipole (ED) moment can be described as:

$$\mathbf{p} = \int_V \varepsilon_0\,(\varepsilon_p - \varepsilon_d)\,\mathbf{E}\,(\mathbf{r}')\,\mathrm{d}\mathbf{r}'. \tag{1}$$

Here, V and $\boldsymbol{r}'$ represent the nanoparticle volume, radius vector of a volume element inside the particle respectively.

The toroidal dipole (TD) moment is expressed as:

$$\mathbf{T} = \frac{i\omega}{10}\int_V \left\{2\mathbf{r}'^2\mathbf{P}\,(\mathbf{r}') - [\mathbf{r}'\cdot\mathbf{P}\,(\mathbf{r}')]\,\mathbf{r}'\right\}\mathrm{d}\mathbf{r}'. \tag{2}$$

The MD moment is given by:

$$\mathbf{m} = -\frac{i\omega}{2}\int_V [\mathbf{r}'\times\mathbf{P}\,(\mathbf{r}')]\,\mathrm{d}\mathbf{r}'. \tag{3}$$

The electric quadrupole and magnetic quadrupole tensors ($\hat{U}$ is the 3×3-unit tensor) are written as:

$$\hat{Q} = 3\int_V \left\{\mathbf{r}'\mathbf{P}\,(\mathbf{r}') + \mathbf{P}\,(\mathbf{r}')\,\mathbf{r}' - \frac{2}{3}\,[\mathbf{r}'\cdot\mathbf{P}\,(\mathbf{r}')]\,\hat{\mathrm{U}}\right\}\mathrm{d}\mathbf{r}'. \tag{4}$$

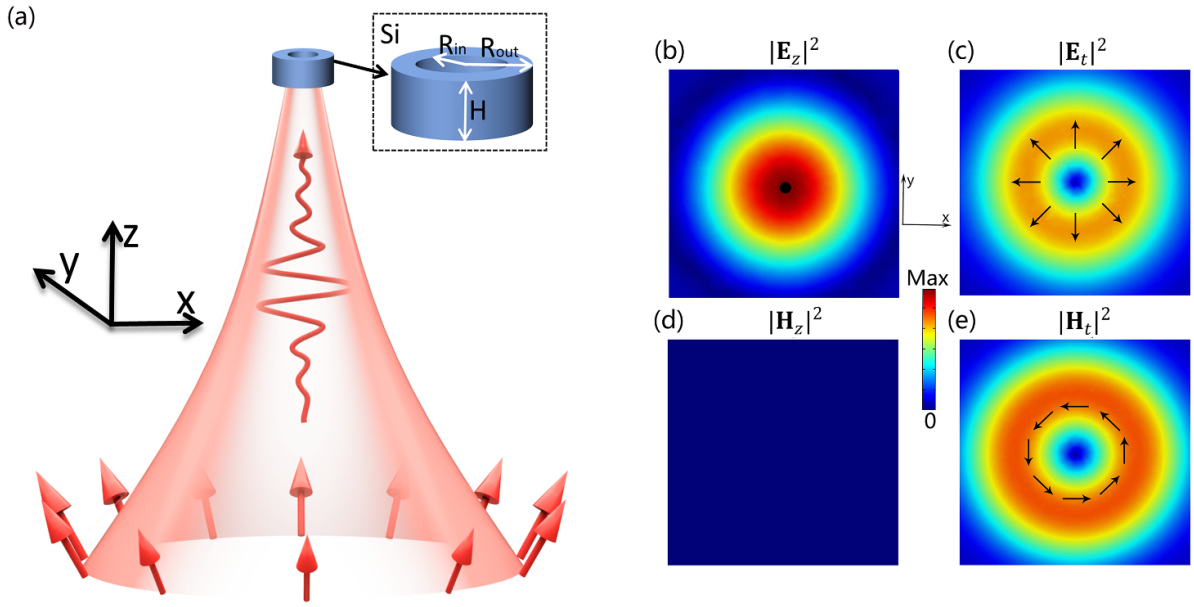

Figure 1. (a) Schematic diagram of the SHND under a tightly focused RPB. (b) Theoretical electromagnetic field intensity distributions $|\mathbf{E}_z|^2$, $|\mathbf{E}_t|^2$, $|\mathbf{H}_z|^2$, $|\mathbf{H}_t|^2$ for the tightly focused RPB.

$$\hat{\mathrm{M}} = \frac{\omega}{3\mathrm{i}} \int_V \{[\mathbf{r}' \times \mathbf{P}(\mathbf{r}')]\,\mathbf{r}' + \mathbf{r}'\,[\mathbf{r}' \times \mathbf{P}(\mathbf{r}')]\}\,\mathrm{d}\mathbf{r}'. \tag{5}$$

The interference of the ED and TD moments can be regarded as the TED moment $\mathbf{TED} = \mathbf{p} + \frac{i\varepsilon_d k_0}{c}\mathbf{T}$ where k_0 and c represent wave numbers and light velocity in vacuum respectively. Then, the total far-field scattering cross section σ_{sca} is the sum of that from all the mentioned multipoles above:

$$\begin{aligned}\sigma_{\mathrm{sca}} = {} & \frac{k_0^4}{6\pi\varepsilon_0^2|E_{\mathrm{inc}}|^2}\left|\boldsymbol{p} + \frac{ik_0\varepsilon_d}{c}\boldsymbol{T}\right|^2 + \frac{k_0^4\varepsilon_d\mu_0}{6\pi\varepsilon_0|E_{\mathrm{inc}}|^2}|m|^2 \\ & + \frac{k_0^6\varepsilon_d}{720\pi\varepsilon_0|E_{\mathrm{inc}}|^2}\sum|Q_{\alpha\beta}|^2 + \frac{k_0^6\varepsilon_d^2\mu_0}{80\pi\varepsilon_0|E_{\mathrm{inc}}|^2} \\ & \times \sum|M_{\alpha\beta}|^2. \end{aligned} \tag{6}$$

Other high order multipoles are neglected here. Where, $\alpha = \mathrm{x}, y, z$, $\beta = \mathrm{x}, y, z$, and μ_0 is the vacuum permeability.

3. Results and discussion

3.1. Broadband transverse unidirectional scattering in the visible region

According to figure 2(a), only the pure broadband total electric TED resonance is excited while the influence of remaining responses on the total scattering is negligible when the SHND is located at the focal point of RPB (i.e. $(x, y) = (0, 0)$ nm in the focal plane). Emphatically, the broad total electric z-dipole (TED_z) generated in the SHND under RPB plays a crucial role in realizing broadband and transverse scattering. The induced TED_z is further confirmed by the strong z-direction electric field in xy cut plane through the center of the SHND, as shown in figure 2(e) where the dotted lines indicate the inner and outer radius of the SHND respectively. Furthermore, we consider that the SHND has a transverse displacement along the x-axis relative to optical axis in the focal plane. Figures 2(b) and (c) show the scattering spectrum when the SHND is located at $x = 180$ nm away from the optical axis of RPB (i.e. $(x, y) = (180, 0)$ nm in the focal plane). It is found that transverse magnetic y- dipole (MD_y) and total electric x-dipole (TED_x) are also induced besides TED_z while the contributions of other components and high-order multipoles are insignificant and can thereby be ignored in this spectrum. According to figures 1(c) and (e) above, transverse magnetic and electric responses are excited when the SHND has a transverse displacement because $\mathbf{H}_t$ and $\mathbf{E}_t$ enhance with the distance away from the optical axis, which is consistent with the scattering spectrum in figure 2(b). Consequently, the far-field radiation is determined by the interference of the TED_z, MD_y and TED_x when the SHND has a transverse displacement along the x-axis relative to optical axis in the focal plane. In addition, according to the far field radiation pattern of the dipoles, the radiation deflection in the x direction is dominated by the interference between TED_z and MD_y. The TED_z and MD_y generate constructive and destructive interference in the $\pm x$ direction if their amplitudes are similar and the phase difference is close to 0 or π (i.e. the two dipoles are considered as in-phase or out-phase) [28, 29]. From figure 2(d), the phase difference φ_1 between TED_z and MD_y is close to π in the wavelength range from 581 nm to 656 nm when the SHND is located at $x = 180$ nm, which provides the possibility to realize transverse unidirectional scattering towards the $-x$ direction.

Figure 3(a) is the scattering schematic diagram of the SHND illuminated by the tightly focused RPB. According to the analysis above, only TED_z resonance is induced when the SHND is located at the focal point, which generates a donut-like shape far-field scattering, namely an evenly distributed scattering in all directions within xy plane, as

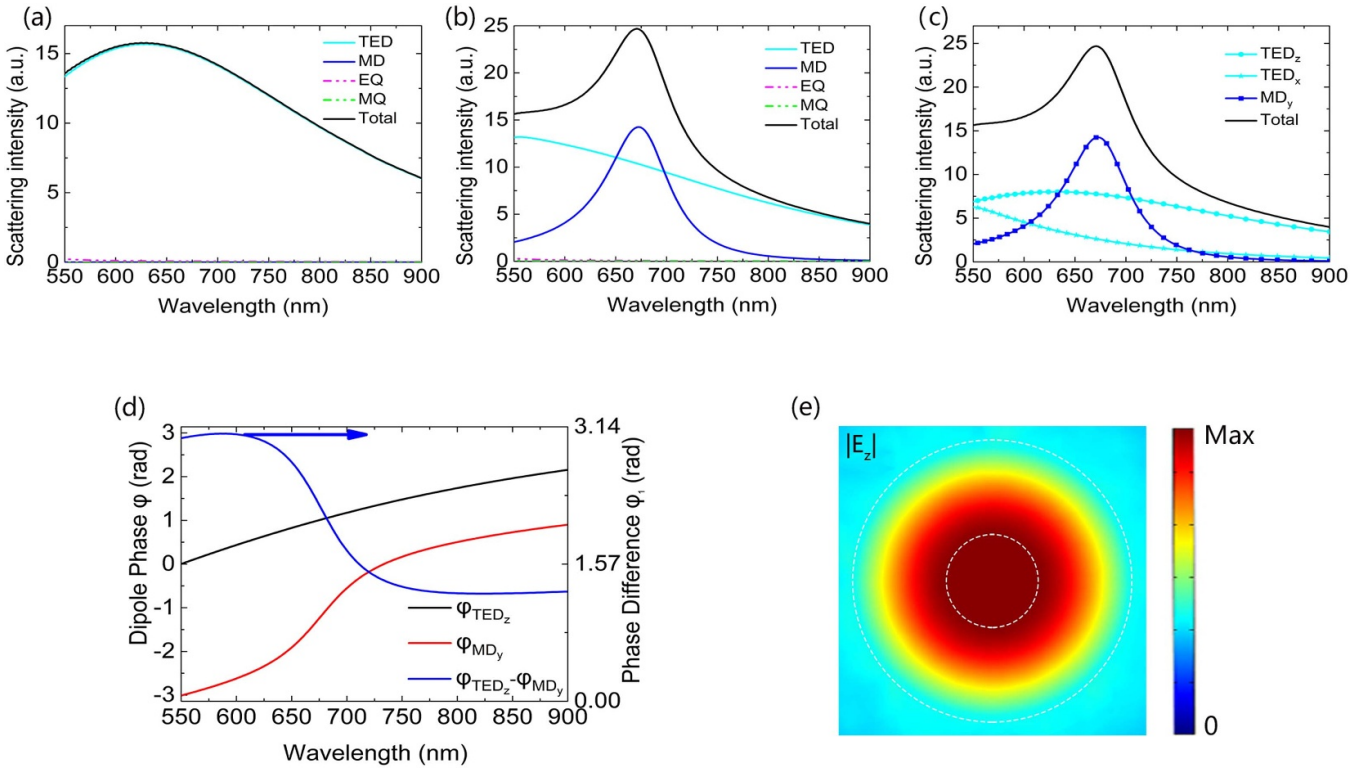

Figure 2. (a) Scattering spectra (total and the contributions from the first two order multipoles) when the SHND is located at $x = 0$ nm. (b) Scattering spectra (total and the contributions from the first two order multipoles), (c) scattering spectra (total and the contributions from TED$_z$, MD$_y$ and TED$_x$) and (d) phase and phase difference φ_1 of TED$_z$ and MD$_y$ when the SHND is located at $x = 180$ nm. (e) Electric field z component intensity $|\mathbf{E}_z|$ in xy cut plane of the SHND at TED resonance.

shown in inset of figure 3(a). According to figure 2(d), there is a phase difference π between TED$_z$ and MD$_y$ in certain wavelength regions when the SHND is located at $x = 180$ nm, leading to the far-field radiation mainly along the $-x$ direction. Additionally, we find that the phase difference φ_2 between TED$_x$ and MD$_y$ is close to $3\pi/2$ in this wavelength range, which means little contribution to the unidirectional radiation along the z-axis. At TED$_z$ resonance wavelength $\lambda = 630$ nm, stronger magnetic field is also excited due to the circle structure of hollow silicon disk, and the phase difference φ_1 between TED$_z$ and MD$_y$ is 0.94 π, leading to a highly-efficient transverse unidirectional scattering along the $-x$ direction, as shown in figure 3(b). As we can see from figure 3(c), the $-x$ direction radiation dominates in the xy plane. In the xz plane (figure 3(d)), the unidirectional radiation deflection in the z direction is not obvious. Similarly, if the SHND is displaced along y-axis, a highly-efficient transverse unidirectional scattering along the y direction can also be realized.

According to the above dipole phase analysis, it is possible to achieve broadband transverse unidirectional scattering. In order to quantitatively describe the unidirectional characteristic of far-field radiation, here, we define a transverse contrast ratio of intensity in the $-x$ direction to that in the $+x$ direction [49]:

$$D_x = \frac{|E_{-x}|^2 - |E_{+x}|^2}{|E_{-x}|^2 + |E_{+x}|^2}. \tag{7}$$

Obviously, $D_x = 1$ means electric field is totally scattered towards the $-x$ direction; $D_x = -1$ means electric field is totally scattered towards the $+x$ direction; and $D_x = 0$ means the scattering towards the $-x$ direction and $+x$ direction is equal. That is, the closer the $|D_x|$ is to 1, the better the unidirectivity. It is found from figure 4(a) that the unidirectivity of transverse unidirectional scattering towards $-x$ direction is best at $\lambda = 630$ nm where D_x reaches 0.90. In addition, the minimum of D_x reaches 0.80 with good unidirectivity in the broadband range of 75 nm from 581 nm to 656 nm, which enables broadband transverse unidirectional scattering in the visible region. The insets exhibit the 3D radiation diagrams at $\lambda = 581$ nm, $\lambda = 605$ nm, $\lambda = 630$ nm, $\lambda = 656$ nm where the far-field radiation towards $+x$ direction is mostly suppressed. Figure 4(b) shows the rightward scattering intensity of the SHND with outer radius R_{out} fixed at 90 nm and R_{in} fixed at 50 nm as the function of the wavelength and height H. It is found that broadband rightward ($+x$ direction) scattering is greatly suppressed in the wavelength range from 581 nm (vertical white dotted line) to 656 nm (vertical white dotted line) when $H = 200$ nm (horizontal white dotted line), mainly resulting from the interference between TED$_z$ and MD$_y$. The red color in figure 4(c) shows that, when zero rightward scattering is achieved, highly enhanced leftward ($-x$ direction) scattering can be obtained in this visible region, corresponding to the dark blue region in figure 4(b). In our paper, the amplitudes of TED$_z$ and MD$_y$ are almost equal at the central wavelength $\lambda = 630$ nm where the contrast ratio D$_x$ reaches 0.90. However,

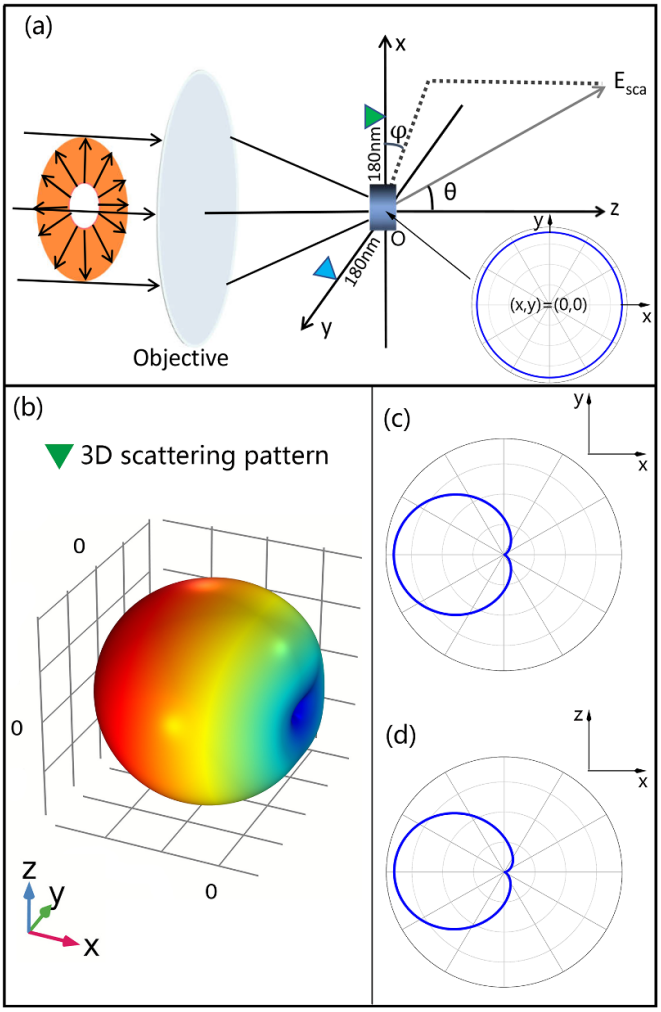

Figure 3. (a) Schematic diagram of light scattering of the SHND illuminated by the RPB (the inset shows 2D radiation pattern in xy cut plane at resonance wavelength when the SHND is located at $x = 0$ nm. (b) 3D radiation pattern, (c) 2D radiation pattern in xy cut plane and (d) 2D radiation pattern in xz cut plane at $\lambda = 630$ nm when the SHND is located at $x = 180$ nm.

the amplitudes of the two dipoles differ at other wavelengths we study, so there is a drop of the contrast ratio D_x at other wavelengths compared with that at the central wavelength. Nevertheless, the contrast ratio D_x at other wavelengths still exceeds 0.80.

To discuss the scattering of different materials, we compare GaAs with Si. Based on previous research, the magnetic resonance is dampened more severely by the imaginary part of the refractive index than the electric resonance [50]. In figure 5(a), it is found that GaAs has a larger imaginary part of refractive index than Si in the visible region, which makes the damping of magnetic resonance is more severe in GaAs than that in Si. Therefore, the wavelength range enclosed by the intersection of electric and magnetic resonance is smaller in the GaAs hollow nanodisk, and the bandwidth of transverse unidirectional scattering in the GaAs hollow nanodisk is narrower than that in the SHND. As we can see from figure 5(b), the broadband range where transverse scattering intensity contrast ratio D_x exceeds 0.80 (horizontal black dotted line) is from 593 nm to 646 nm and the bandwidth is 53 nm for the GaAs hollow nanodisk. In the SHND, the corresponding bandwidth is 75 nm which is wider than 53 nm in the GaAs hollow nanodisk because of the smaller imaginary part of refractive index of Si.

3.2. Unidirectional angular radiation controlled by the position of the SHND

According to the above discussion, TED_z and MD_y are dominant in the scattering spectrum when the SHND has a transverse displacement along the x-axis relative to optical axis in the focal plane. The interference between the two dipoles induces transverse scattering along the x-axis, as shown in figure 6(g) where the black and pink line represent 2D radiation patterns when the phase difference between TED_z and MD_y is π and 0 respectively. Figures 6(a)–(f) show the 3D and 2D radiation patterns of the MD_y, TED_z and MD_x. Similar to the situation where TED_z and MD_y interfere, it is found that the far-field radiation deflection in the y direction is dominated by the interference between TED_z and MD_x in figures 6(d) and (f). In figure 6(h), the cyan and orange line represent 2D radiation patterns when the phase difference between TED_z and MD_y is 0 and π respectively. There is a net constructive interference in the $+y$ direction while destructive interference in the $-y$ direction if the phase difference between TED_z and MD_y is 0. Similarly, there is a net constructive interference in the $-y$ direction while destructive interference in the $+y$ direction if the phase difference between TED_z and MD_y is π. In summary, the far-field radiation deflection towards $\pm x$ or $\pm y$ direction is collectively referred to as transverse unidirectional scattering. Furthermore, the combination of the radiation deflection towards $\pm x$ and $\pm y$ direction makes the unidirectional angular radiation deflect towards various directions. For example, in figure 6(i), the olive line represents the combination of the radiation deflection towards $-x$ and $-y$ direction, and the magenta line represents the combination of the radiation deflection towards $+x$ and $-y$ direction. In these cases, MD_y and MD_x interfere with TED_z simultaneously.

Figure 7 depicts that the different positions of the SHND relative to the focal point O (0, 0) of RPB cause unidirectional angular radiation to deflect towards different directions. Here, we define the azimuth angle of O (0, 0) relative to the SHND position (x, y) as θ, where $\tan\theta = y/x$. For example, $\theta = 180°$ when the SHND is located at $(x, y) = (180, 0)$ nm and $\theta = 270°$ when the SHND is located at $(x, y) = (0, 180)$ nm, as shown in figure 7(a). We also define the far-field radiation angle as ϕ. According to figure 3 above, if the SHND is located at $\theta = 180°$, the interference between TED_z and MD_y leads to unidirectional angular radiation deflecting towards $-x$, i.e. $\phi = 180°$; In the same way, if the SHND is located at $\theta = 270°$, the interference between TED_z and MD_x leads to unidirectional angular radiation deflecting towards $-y$, i.e. $\phi = 270°$, as shown in figure 7(d). In the same way, when $\theta = 0°$ or $\theta = 90°$, the constructive interference between TED_z and MD_y/MD_x leads to unidirectional angular radiation deflecting towards $+x$ or $+y$ direction, i.e. $\phi = 0°$ or $\phi = 90°$,

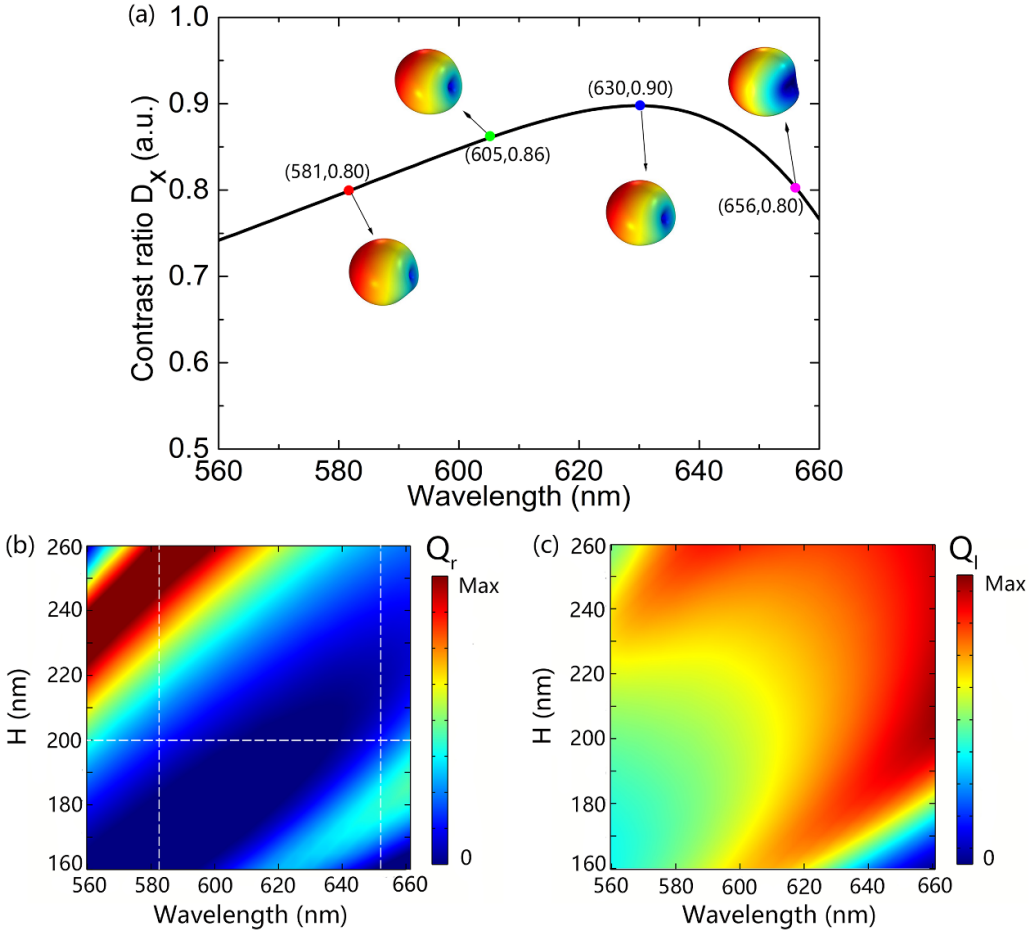

Figure 4. (a) Transverse scattering intensity contrast ratio D_x as a function of wavelength when the SHND is located at $x = 180$ nm. The insets show 3D radiation patterns at $\lambda = 581$ nm, $\lambda = 605$ nm, $\lambda = 630$ nm, $\lambda = 656$ nm. (b) Contour plot of the rightward ($+x$ direction) scattering intensity as a function of wavelength and height H. (c) Contour plot of the leftward ($-x$ direction) scattering intensity as a function of wavelength and height H.

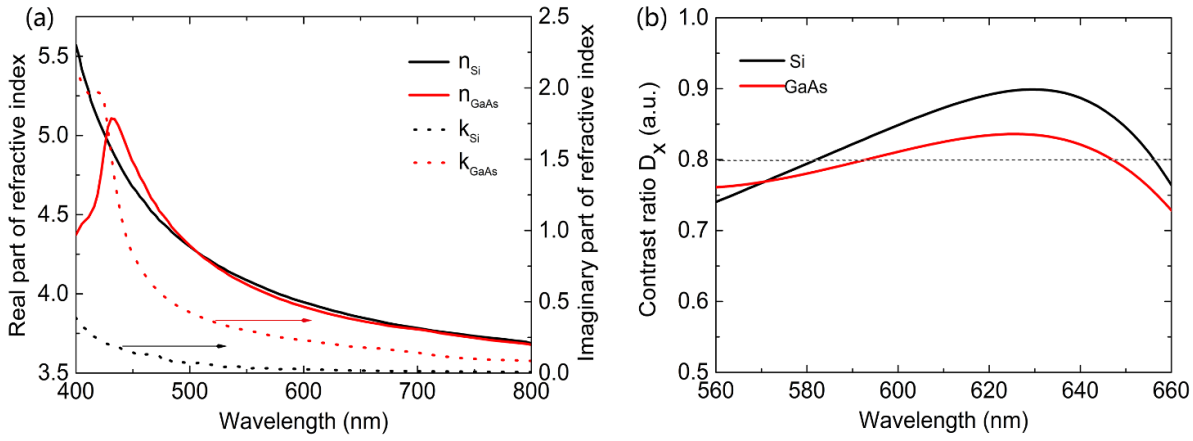

Figure 5. (a) The refractive index of Si and GaAs. (b) Transverse scattering intensity contrast ratio D_x as a function of wavelength when the Si or GaAs hollow nanodisk is located at $x = 180$ nm.

as shown in figures 7(c) and (e). According to the ideas above, we consider that if the SHND is located at $(x, y) = (180, 180)$ nm (i.e. $\theta = 225°$), TED_z interferes with MD_y and MD_x simultaneously, and the angular radiation deflection towards $-x$ and $-y$ direction is exactly the same. Therefore, the angular radiation deflects towards $-x$ and $-y$ direction by 45° respectively, that is, $\phi = 225°$. Similarly, if the SHND is located at $(x, y) = (-180, -180)$ nm (i.e. $\theta = 45°$), the angular radiation deflects towards $+x$ and $+y$ direction by 45° respectively, that is, $\phi = 45°$, which is consistent with the simulation results in

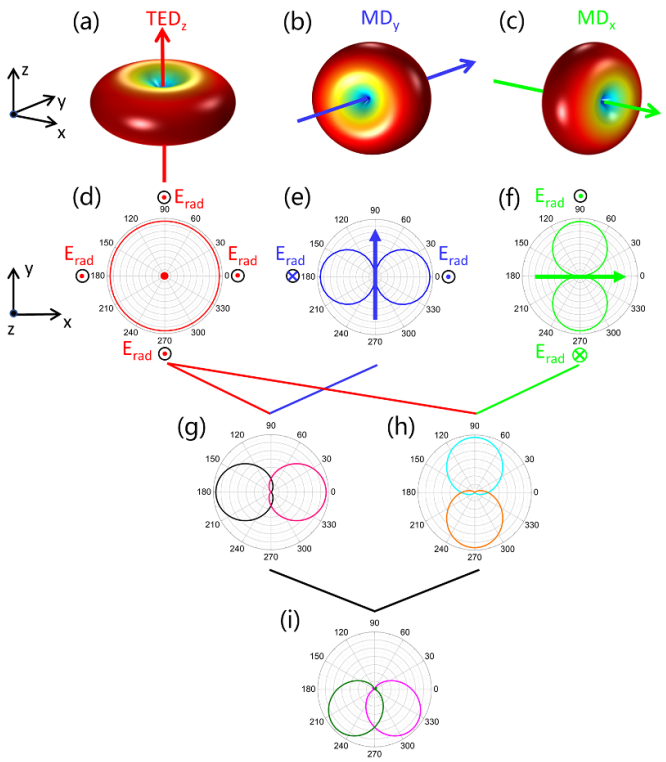

Figure 6. (a)–(c) Schematic diagram depicting the 3D radiation patterns of TED$_z$, MD$_y$, and MD$_x$ induced in the nanoparticle. (d)–(f) Schematic diagram depicting the 2D radiation patterns of TED$_z$, MD$_y$, and MD$_x$ induced in the nanoparticle. (g), (h) The radiation pattern based on the interference between TED$_z$ and MD$_y$ and that based on the interference between TED$_z$ and MD$_x$. (i) The radiation pattern resulting from the interference of these three dipoles.

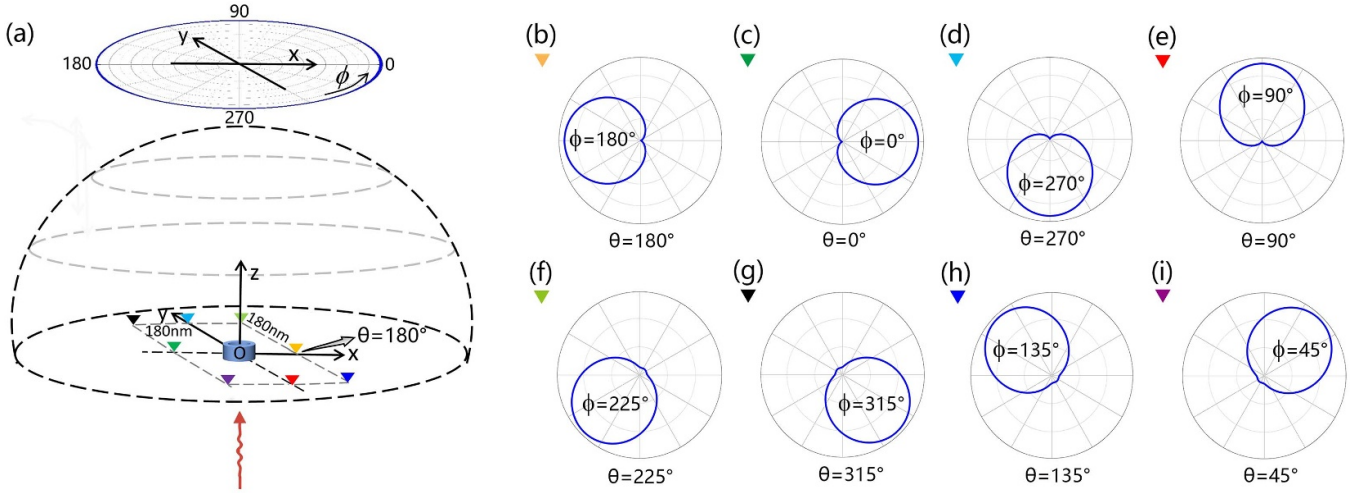

Figure 7. (a) Schematic diagram of the SHND moving on the xy plane, illuminated by RPB along the $+z$ direction. (b)–(i) The 2D radiation pattern in xy cut plane of the SHND at different positions.

figures 7(f) and (i). In the same way, the corresponding results $\phi = 135°$ and $\phi = 315°$ are obtained when the SHND is located at $(x, y) = (180, -180)$ nm and $(x, y) = (-180, 180)$ nm respectively, as shown in figures 7(g) and (h). The above results show that ϕ corresponds to θ one to one, which means angular radiation can be adjusted in various directions by changing the position of the SHND in the focal plane.

Furthermore, we discuss the unidirectional angular radiation regulation in more detail. We fix $x = 180$ nm and make y vary from -180 nm to $+180$ nm, i.e. $\theta = 135°\sim225°$. The induced MD$_y$ and MD$_x$ interfere with TED$_z$ at different levels when the displacement of the SHND in the x direction is greater than that in the y direction, such as $(x, y) = (180, 90)$ nm (i.e.,$\theta = 207°$), and the angular radiation is deflected towards $-x$ axis and away from $-y$ axis with the simulation result $\phi = 207°$. This result further confirms that θ and ϕ are always approximately equal. Therefore, when $x = 180$ nm is fixed, the angular radiation direction can be

adjusted in 90° range from 135° to 225° by changing the position of the SHND. Similarly, for the other three cases where $x = -180$ nm (i.e. $\theta = 0° \sim 45°, \theta = 315° \sim 360°$), $y = 180$ nm (i.e. $\theta = 225° \sim 315°$), and $y = -180$ nm (i.e. $\theta = 45° \sim 135°$) are fixed, θ and ϕ are still approximately equal. Therefore, we can draw the conclusion that 360° unidirectional angular radiation can be achieved by adjusting the position of the SHND in the focal plane. In addition, we also find above unidirectional angular radiation regulation can be realized in the visible broadband range, which makes up for the previous limitation that radiation direction is strongly dependent on incident wavelength.

4. Conclusion

In conclusion, we use the SHND illuminated by a tightly focused RPB to realize the manipulated unidirectional scattering in the transverse direction in the visible region. The induced TED_z interfere with MD_y at resonance when the SHND is located at a specific position, which makes the highly-efficient transverse unidirectional scattering realized. In addition, the transverse unidirectional scattering with a broad wavelength range from 581 nm to 656 nm can be realized. Finally, our results show that the unidirectional angular radiation towards all directions can be realized by adjusting the position of the SHND. Our findings above have potential applications in fields such as optical communications, photovoltaic technology, biological testing and metasurface.

Data availability statement

The data that support the findings of this study are available upon reasonable request from the authors.

Acknowledgments

This work was supported by Natural Science Foundation of Guangdong Province, China (Grant Nos. 2018A030313854 and 2019A1515011578); Science and Technology Program of Guangzhou (Grant No. 2019050001); National Nature and Science Foundation of China (Grant No. 11874020).

ORCID iD

Haiying Liu https://orcid.org/0000-0002-5280-1892

References

[1] Smirnova D and Kivshar Y S 2016 *Optica* **3** 1241–55
[2] Guo Y, Pu M, Li X, Ma X, Song S, Zhao Z and Luo X 2018 *IEEE J. Sel. Top. Quantum Electron.* **24** 4700107
[3] Guo Y, Pu M, Li X, Ma X and Luo X 2018 *Appl. Phys. Express* **11** 092202
[4] Vercruysse D, Neutens P, Lagae L, Verellen N and Dorpe P 2017 *ACS Photonics* **4** 1398–402
[5] Bontempi N, Chong K E, Orton H W, Staude I, Choi D Y, Alessandri I, Kivshar Y S and Neshev D N 2017 *Nanoscale* **9** 4972–80
[6] Yan J, Liu P, Lin Z and Yang G 2016 *Nanoscale* **8** 5996–6007
[7] Decker M, Staude I, Falkner M, Dominguez J, Neshev D N, Brener I, Pertsch T and Kivshar Y S 2015 *Adv. Opt. Mater.* **3** 813–20
[8] Yang L, Wu D, Liu Y, Liu C, Xu Z, Li H, Yu Z, Yu L and Ye H 2018 *Photon. Res.* **6** 517–24
[9] Liu L, Ge L, Hu P, Xiang H, Yang W, Liu Q and Han D 2018 *J. Phys. D: Appl. Phys.* **51** 035106
[10] Maharana P K, Srivastava T and Jha R 2014 *J. Phys. D: Appl. Phys.* **47** 385102
[11] Vercruysse D, Zheng X, Sonnefraud Y, Verellen N, Martino G D, Lagae L, Vandenbosch G A E, Moshchalkov V V, Maier S A and Dorpe P V 2014 *ACS Nano* **8** 8232–41
[12] Novin S, Sadatgol M, Zarrabi F and Bazgir M 2019 *Optik* **176** 14–23
[13] Jahangiria P, Zarrabib F, Moghadasia M, Arezoomandc A and Heydari S 2017 *Opt. Commun.* **394** 80–85
[14] Fang Z, Zhen Y, Fan L, Zhu X and Nordlander P 2012 *Phys. Rev.* B **85** 245401
[15] Fu Y H, Kuznetsov A I, Miroshnichenko A E, Yu Y F and Luk'yanchuk B 2013 *Nat. Commun.* **4** 1527
[16] Ma C, Yan J, Huang Y and Yang G 2019 *Small* **15** 1900546
[17] Yao K and Liu Y 2016 *ACS Photonics* **3** 953–63
[18] Geffrin J M *et al* 2012 *Nat. Commun.* **3** 1171
[19] García-Etxarri A, Gómez-Medina R, Froufe-Pérez L S, López C, Chantada L, Scheffold F, Aizpurua J, Nieto-Vesperinas M and Sáenz J J 2011 *Opt. Express* **19** 4815–26
[20] Makarov S V *et al* 2017 *Nano Lett.* **17** 3047–53
[21] Smirnova D, Smirnov A I and Kivshar Y S 2018 *Phys. Rev.* A **97** 013807
[22] Kerker M, Wang D S and Giles C L 1983 *J. Opt. Soc. Am.* **73** 765–7
[23] Liu W and Kivshar Y 2018 *Opt. Express* **26** 13085–105
[24] Li R, Zhou X, Panmai M, Xiang J, Liu H, Ouyang M, Fan H, Dai Q and Wei Z 2018 *Opt. Express* **26** 28891–901
[25] Shamkhi H K, Baryshnikova K V, Sayanskiy A, Kapitanova P, Terekhov P D, Belov P, Karabchevsky A, Evlyukhin A B, Kivshar Y and Shalin A S 2019 *Phys. Rev. Lett.* **122** 193905
[26] Shamkhi H K, Sayanskiy A, Valero A C, Kupriianov A S, Kapitanova P, Kivshar Y, Shalin A S and Tuz V R 2019 *Phys. Rev. Mater.* **3** 85201
[27] Li J, Verellen N, Vercruysse D, Bearda T, Lagae L and Dorpe P V 2016 *Nano Lett.* **16** 4396–403
[28] Panmai M, Xiang J, Sun Z, Peng Y, Liu H, Liu H, Dai Q, Tie S and Lan S 2018 *Opt. Express* **26** 12344–62
[29] Tian J, Li Q, Yang Y and Qiu M 2016 *Nanoscale* **8** 4047–53
[30] Youngworth K S and Brown T G 2000 *Opt. Express* **7** 77–87
[31] Deng F, Liu H, Panmai M and Lan S 2018 *Opt. Express* **26** 20051–62
[32] Bag A, Neugebauer M, Wozniak P, Leuchs G and Banzer P 2018 *Phys. Rev. Lett.* **121** 193902
[33] Xu J, Fan H, Dai Q, Liu H and Lan S 2021 *J. Phys. D: Appl. Phys.* **54** 215102
[34] Zhang D, Xiang J, Liu H, Deng F, Liu H, Ouyang M, Fan H and Dai Q 2017 *Opt. Express* **25** 26704–13
[35] Liu W, Miroshnichenko A E, Neshev D N and Kivshar Y S 2012 *ACS Nano* **6** 5489–97
[36] Novotny L and Hulst N 2011 *Nat. Photon.* **5** 83–90
[37] Neugebauer M, Bauer T, Banzer P and Leuchs G 2014 *Nano Lett.* **14** 2546–51
[38] Isro S D, Iskandar A A, Kivshar Y S and Shadrivov I V 2018 *Opt. Express* **26** 32624–30
[39] Yu H, Zhu H, Li J, Cao Z and Chen H 2021 *Crystals* **11** 920–8

[40] Urbach H P and Pereira S F 2008 *Phys. Rev. Lett.* **100** 123904
[41] Quabis S, Dorn R, Eberler M, Glockl O and Leuchs G 2000 *Opt. Commun.* **179** 1–7
[42] Palik E D 1985 *Handbook of Optical Constants of Solids* (New York: Academic)
[43] Tuz V, Khardikov V and Kivshar Y S 2018 *ACS Photonics* **5** 1871
[44] Liu X, Li J, Zhang Q and Wang Y 2020 *Opt. Lett.* **45** 2826
[45] Richards B and Wolf E 1959 *Proc. R. Soc. Lond.* A **253** 358–79
[46] Novotny L and Hecht B 2012 *Principles of Nano-optics* (Cambridge: Cambridge University Press)
[47] Miroshnichenko A E, Evlyukhin A B, Yu Y F, Bakker R M, Chipouline A, Kuznetsov A I, Luk'yanchuk B, Chichkov B N and Kivshar Y S 2015 *Nat. Commun.* **6** 8069
[48] Evlyukhin A B, Fischer T, Reinhardt C and Chichkov B N 2016 *Phys. Rev.* B **94** 205434
[49] Wang Y, Lu Y and Wang P 2018 *Opt. Express* **26** 1000–11
[50] Ma C, Yan J, Huang Y and Yang G 2017 *Adv. Opt. Mater.* **5** 1700761